Hindawi
Shock and Vibration
Volume 2022, Article ID 8200199, 15 pages
https://doi.org/10.1155/2022/8200199

Research Article

Damage Identification of Wind-Break Wall Structures based on the Further Updated Wavelet Packet Frequency Bands Energy Ratio Spectrum

Qian Xu

School of Civil Engineering and Architecture, Shaanxi University of Technology, Hanzhong 723001, Shaanxi, China

Correspondence should be addressed to Qian Xu; xuqian20121601014@163.com

Received 15 April 2022; Accepted 23 June 2022; Published 19 July 2022

Academic Editor: Yi Qin

Damage will appear in the wind-break wall under the effects of many factors. The wind-break wall may be destroyed when the damage is accumulated to some extent, which may cause accidents. To identify damage within the wind-break wall structure, the Wavelet Packet frequency bands energy ratio spectrum analysis of the virtual impulse response function of responses to the wind-break wall was performed under the effects of excitation. Based on the damage sensitivity analysis of subfrequency bands, a further updated Wavelet Packet frequency bands energy ratio spectrum was proposed. To reflect the damage information sensitively, the feature bands, which were more sensitive to damage, were selected via the threshold value ε_0. Then, the Wavelet Packet damage feature vector and damage identification index, which can reflect damage information of the wind-break walls sensitively, were proposed. A damage identification method for wind-break walls was proposed. To verify the validity of this damage identification method, the vibration tests on a pile plate wind-break wall were performed. Damage within the wall was identified via the method. The tests results show that the damage feature vector is a zero vector and the value of damage index is zero, when the wind-break wall is not damaged. The damage feature vector is a nonzero vector and the value of damage index is positive, when the wind-break wall is damaged. Thus, the damage state of the wind-break wall can be detected via the damage feature vector and damage index. With increase of damage accumulated within the wall, the damage intensity and the value of the damage index increase. The quantitative relationship between the damage index and damage intensity is established. The damage intensity can be calculated reversely, when the damage index is available. Thus, the damage intensity of the wind-break wall can be identified via the quantitative relationship between the damage index and damage intensity. In addition, the damage index value of the measuring point, which is much closer to the partial damage, is much larger. The damage index value of the point, which is located at the partial damage, is the largest. Thus, the damage location of the wind-break wall can be diagnosed via the characteristics of damage index for different measurement points. Thus, the damage state, damage location, and damage intensity of the wind-break wall can be identified via this damage identification method.

1. Introduction

The wind-break wall structures, which were mainly used to resist the wind, stabilize the sand, protect the train, and withstand the wind and wave, were widely applied in railway engineering, highway engineering, ocean engineering, and so forth. To protect the train from strong wind and sand, hundreds of miles of wind-break walls were built along the Lanzhou-Xinjiang high-speed railway in the strong wind area in China [1]. However, under such effects as wind-sand erosion, material aging, climate change, and load variation, such damage as the concrete crack of the wind-break wall and cementation failure between steels and concrete would appear and accumulate continuously in the wall. For instance, the concrete of wind-break walls always cracked prematurely under the effects of high temperature, large temperature difference, and wind-sand erosion in the Turpan area of Lanzhou-Xinjiang high-speed railway [2]. The accumulated damage might cause partial destruction and collapse of the wall when the damage is accumulated to

some extent, which would reduce the protective capability of the wall. In particular, the destruction or failure of the wind-break wall would reduce the protective capability of the wall in the strong wind area, which might cause such accidents as interruption of the running train and even derailment of the train [3]. In addition, the sand and stone, which moved through the wind-break wall with damage, might hit the running train with high speed or pile upon the railway. This would affect the safety of train seriously. Consequently, it is necessary to conduct health monitor for the wind-break wall and repair the damage within the wall in time so as to avoid or decrease accidents.

Nowadays, most research works on wind-break wall structures are listed as follows: (1) The characteristics of resisting winds about wind-break walls and the dynamic response regularities of the coupled air between the running train and wind-break walls were investigated. For instance, Li et al. studied the dynamic response regularities of the coupled air between the Electric Multiple Unit train and wind-break walls with different height via the wind tunnel tests, and the efficiencies of resisting winds about wind-break walls were also compared [4]. Han et al. analyzed the structural characteristics of wind-sand flow of wind-break walls in strong wind area via the field tests and numerical simulations [5]. (2) Dynamic response regularities of wind-break wall structures and the deposition mechanism of the sand behind the wind-break walls were investigated under the effects of wind-sand flow. For example, Xin et al. analyzed the movement characteristics of wind-sand in either side of the wind-break wall along the Lanzhou-Xinjiang high-speed railway via the numerical simulations. The distribution characteristics of flow field and deposition regularities of the sand behind the wind-break walls were acquired [6]. Cheng et al. investigated the efficiencies of resisting winds and deposition regularities of the sand about single wind-break walls and double ones via the wind tunnel tests [7]. The reasonable type, height, thickness, and distance of the wind-break walls were investigated under the effects of wind-sand flow and running trains with high speed. Ye and Li et al. analyzed the influences of different types and heights of the wind-break walls on the distribution regularities of sand under the effects of wind and running trains with high speed [8]. Niu and Du investigated the influences of the height and distance of wind-break walls on the efficiencies of resisting wind in high-speed railway. The optimal height and distance of wind-break walls were obtained [9]. However, the investigation of the damage identification for wind-break walls is rare at present.

So far, the research works of damage identification on civil engineering structures are mainly focused on the structural components, building structures, bridge structures, and so forth. For instance, Martin et al. studied the effects of damage on the inherent parameters of a beam via the laboratory tests and numerical simulations. The damage of the beam was identified precisely via the changes of modal parameters [10]. Fu et al. proposed a damage identification method, which was based on the finite element model updating, to diagnose damage within plate structures with consideration of the influences of time-frequency dynamic responses on sensitivity to damage parameters. The results showed that damage could be localized validly and precisely via this method [11]. Based on the element strain energy and modal sensitivity analysis, Zhang et al. identified the damage location and damage intensity of a pile via the variation rate of modal strain energy [12]. On the basis of genetic algorithm, Li proposed an updated damage identification method to identify damage within a three-story frame structure. The results indicated that the damage location and damage intensity could be detected at the same time via this method [13]. Wang et al. proposed a damage alarming index based on the statistical Wavelet Packet energy spectrum via combination of ambient excitation technology and Wavelet Packet analysis, and this alarming index was used to diagnose and alarm the damage within Yangluo River Bridge in Wuhan of China [14]. Jiao et al. proposed a damage identification method to detect damage within bridge structures based on the Chebyshev polynomial fitting and fuzzy logic, when the test information is incomplete [15]. Liu et al. proposed a damage identification method to diagnose damage within urban overpass based on the processing structural static characteristics and dynamic ones via the genetic algorithm [16]. Based on the Wavelet Packet frequency bands energy spectrum analysis of the virtual impulse response function of structural dynamic responses to a retaining wall, Xu proposed a damage identification method for retaining wall structures. The damage state, damage intensity, and damage location could be identified via this method [17]. However, the number of research works on damage identification for wind-break wall structures is much less.

Given lack of research works on health diagnosis and safety alarming for wind-break wall structures at present, the Wavelet Packet frequency bands energy ratio spectrum analysis of virtual impulse response function of dynamic responses to the wind-break wall is performed in this paper. A further updated Wavelet Packet frequency bands energy ratio spectrum is proposed with consideration of the influences of the damage sensitivity of subbands, and the damage feature vector and damage identification index are created. Based on the damage feature vector and damage index, a damage identification method for wind-break wall is proposed. To verify the validity of this damage identification method, damage within a pile plate wind-break wall is diagnosed via tests.

2. Damage Identification Methods

In the light of the research in [18], in comparison with VIRF (the Virtual Impulse Response Function of structural dynamic responses) between the damaged structure and undamaged one, the damage information can be selected. Thus, the Wavelet Packet frequency bands energy spectrum analysis of VIRF is performed to extract damage information.

2.1. The Further Updated Wavelet Packet Frequency Bands Energy Ratio Spectrum. The Wavelet Packet Transforms of h_u and h_d are performed, respectively, and h_u and h_d can be expressed as

$$\begin{cases} h_u = \left[h_{1u,r}\, h_{2u,r} \cdots h_{ju,r} \cdots h_{2^i u,r} \right]^T \\ h_d = \left[h_{1d,r}\, h_{2d,r} \cdots h_{jd,r} \cdots h_{2^i d,r} \right]^T \end{cases}, (r = 1,2,3,\ldots l), \quad (1)$$

where i is the number of Wavelet Packet decomposition orders, l is the number of signal sample points, $h_{ju,r}$ and $h_{jd,r}$ are signal components, and h_u and h_d are response signals of undamaged wind-break wall and damaged one, respectively.

According to the Wavelet Packet frequency bands energy spectrum theory [19], the subfrequency bands energies E_{ju} and E_{jd} can be expressed as

$$\begin{cases} E_{ju} = \sum \left| h_{ju,r} \right|^2 \\ E_{jd} = \sum \left| h_{jd,r} \right|^2 \end{cases}, \quad (2)$$

where E_{ju} and E_{jd} are the subband energies of $h_{ju,r}$ and $h_{jd,r}$, respectively.

Then, the Wavelet Packet frequency bands spectrums $\mathbf{E}_u$ and $\mathbf{E}_d$ can be calculated and expressed as

$$\begin{cases} E_u = \left[E_{1u} \;\; E_{2u} \;\; \cdots \;\; E_{ju} \;\; \cdots \;\; E_{2^i u} \right]^T \\ E_d = \left[E_{1d} \;\; E_{2d} \;\; \cdots \;\; E_{jd} \;\; \cdots \;\; E_{2^i d} \right]^T \end{cases}, \quad (3)$$

where $\mathbf{E}_u$ and $\mathbf{E}_d$ are the initial Wavelet Packet frequency bands energy spectrums of h_u and h_d, respectively.

To reflect energy distribution characteristics of bands with different frequencies, new frequency-ordered energy spectrums are obtained via sorting from low frequency to high one. Then, the frequency-ordered Wavelet Packet frequency bands energy spectrums $\mathbf{E}(\omega)_u$ and $\mathbf{E}(\omega)_d$ can be expressed as

$$\begin{cases} E(\omega)_u = \left[E_{\omega 1u} \;\; E_{\omega 2u} \;\; \cdots \;\; E_{\omega ju} \;\; \cdots \;\; E_{\omega 2^i u} \right]^T \\ E(\omega)_d = \left[E_{\omega 1d} \;\; E_{\omega 2d} \;\; \cdots \;\; E_{\omega jd} \;\; \cdots \;\; E_{\omega 2^i d} \right]^T \end{cases}, \left(\omega_j < \omega_{j+1} \right). \quad (4)$$

In the light of literature [18], damage will cause changes of subfrequency bands energies. In comparison with $\mathbf{E}(\omega)_u$ and $\mathbf{E}(\omega)_d$, damage information can be acquired. $\mathbf{E}(\omega)_u$ and $\mathbf{E}(\omega)_d$ can be used to reflect damage information from absolute energy perspective. However, such relative energy index as energy ratio is always used to reflect damage information [17, 18]. Thus, the energy ratio is defined as

$$\begin{cases} ER_{ju} = \dfrac{E_{\omega ju}}{\sum_{j=1}^{2^i} E_{\omega ju}}, \\ ER_{jd} = \dfrac{E_{\omega jd}}{\sum_{j=1}^{2^i} E_{\omega jd}}. \end{cases} \quad (5)$$

Then, the frequency-ordered Wavelet Packet frequency bands energy ratio spectrums $\mathbf{ER}(\omega)_u$ and $\mathbf{ER}(\omega)_d$ are obtained and expressed as

$$\begin{cases} \mathbf{ER}(\omega)_u = \left[ER_{\omega 1u}\, ER_{\omega 2u} \cdots ER_{\omega ju} \cdots ER_{\omega 2^i u} \right]^T, \\ \mathbf{ER}(\omega)_d = \left[ER_{\omega 1d}\, ER_{\omega 2d} \cdots ER_{\omega jd} \cdots ER_{\omega 2^i d} \right]^T. \end{cases} \quad (6)$$

In comparison with $\mathbf{ER}(\omega)_u$ and $\mathbf{ER}(\omega)_d$, damage information can be acquired.

In the light of literature [17], not all the subfrequency bands can be used to detect structural damage. Generally speaking, only those bands with larger energy can reflect damage information effectively under such interferences as structural inherent frequencies, excitation frequencies, measurement noise, and so forth. Thus, $\mathbf{ER}(\omega)_u$ and $\mathbf{ER}(\omega)_d$ are sorted from large energy value to small one. Then the energy-ordered Wavelet Packet frequency bands energy ratio spectrums $\mathbf{ER}_U$ and $\mathbf{ER}_D$ are proposed and expressed as

$$\begin{cases} \mathbf{ER}_U = \left[ER_{1U} \;\; ER_{2U} \;\; \cdots \;\; ER_{JU} \;\; \cdots \;\; ER_{2^i U} \right]^T, \\ \mathbf{ER}_D = \left[ER_{1D} \;\; ER_{2D} \;\; \cdots \;\; ER_{JD} \;\; \cdots \;\; ER_{2^i D} \right]^T, \end{cases} \quad (7)$$

where $ER_{JU} \geq ER_{(J+1)U}$, $ER_{JD} \geq ER_{(J+1)D}$.

Due to the fact that only partial subbands are useful for damage identification, to select these useful subbands, the relative accumulative energy ratio η is introduced and defined as

$$\eta = \frac{\sum_{J=1}^{P} ER_{JU}}{\sum_{J=1}^{2^i} ER_{JU}} \times 100\% \; (0 \leq \eta \leq 100\%). \quad (8)$$

The first P subbands can be selected from $\mathbf{ER}_U$ to reflect damage information, when $\eta \geq \eta_0$ (η_0 is a threshold value). The residual $(2^i - P)$ subbands are merged into one band, which is called residual band and defined as the $(P+1)^{\text{th}}$ band with consideration of damage information completeness. Then updated Wavelet Packet frequency bands energy ratio spectrums $\mathbf{ER}_{(P+1)U}$ and $\mathbf{ER}_{(P+1)D}$ are proposed and expressed as

$$\begin{cases} \mathbf{ER}_{(P+1)U} = \left[ER_{1U} \;\; ER_{2U} \;\; \cdots \;\; ER_{PU} \;\; ER_{(P+1)U} \right]^T, \\ \mathbf{ER}_{(P+1)D} = \left[ER_{1D} \;\; ER_{2D} \;\; \cdots \;\; ER_{PD} \;\; ER_{(P+1)D} \right]^T, \end{cases} \quad (9)$$

where $ER_{(P+1)U} = 1 - \sum_{J=1}^{P} ER_{JU}$, $ER_{(P+1)D} = 1 - \sum_{J=1}^{P} ER_{JD}$.

Nevertheless, those bands with larger energies may be not necessarily sensitive to damage. Thus, reflecting damage information via those bands with larger damage sensitivity should be more reasonable. To select those bands with stronger damage sensitivity, the ratio of energy ratio deviation ε is introduced and defined as

$$\varepsilon = \frac{\left| ER_{JU} - ER_{JD} \right|}{\left| ER_{JU} - ER_{JD} \right|_{\max}} \; (0 \leq \varepsilon \leq 1). \quad (10)$$

The damage sensitivity of each subband can be evaluated via ε. The value of ε is much larger, and the damage sensitivity of the subband is much stronger. Thus, $\mathbf{ER}_{(P+1)U}$ and $\mathbf{ER}_{(P+1)D}$ are sorted again from large ε value to small one. Then further updated Wavelet Packet frequency bands energy ratio spectrums $\underline{\mathbf{ER}}_{(P+1)U}$ and $\underline{\mathbf{ER}}_{(P+1)D}$ are proposed and expressed as

$$\begin{cases} \underline{\mathbf{ER}}_{(P+1)U} = \left[\underline{ER}_{1U} \;\; \underline{ER}_{2U} \;\; \cdots \;\; \underline{ER}_{PU} \;\; \underline{ER}_{(P+1)U} \right]^T, \\ \underline{\mathbf{ER}}_{(P+1)D} = \left[\underline{ER}_{1D} \;\; \underline{ER}_{2D} \;\; \cdots \;\; \underline{ER}_{PD} \;\; \underline{ER}_{(P+1)D} \right]^T, \end{cases} \quad (11)$$

where $\underline{\mathbf{ER}}_{(P+1)U}$ and $\underline{\mathbf{ER}}_{(P+1)D}$ are the further updated Wavelet Packet frequency bands energy ratio spectrums of h_u and h_d, respectively.

However, the effects of those bands with poorer damage sensitivity on damage identification are much weaker. To reflect the damage information more effectively, the first $Q(Q \le (P+1))$ bands are extracted from the further updated Wavelet Packet frequency bands energy ratio spectrum, when $\varepsilon \ge \varepsilon_0$ (ε_0 is a threshold value). These Q bands can be used to reflect the damage information more effectively. The residual $((P+1)-Q)$ bands are merged into the $(Q+1)^{\text{th}}$ band which is called additional band with consideration of damage information completeness, and these $(Q+1)$ frequency bands are defined as feature frequency bands. Then, the Wavelet Packet feature vectors $\underline{\mathbf{ERV}}_U$ and $\underline{\mathbf{ERV}}_D$ are created and expressed as

$$\begin{cases} \underline{\mathbf{ERV}}_U = \left[\underline{ERV}_{1U}\ \underline{ERV}_{2U} \cdots \underline{ERV}_{QU}\ \underline{ERV}_{(Q+1)U} \right]^T, \\ \underline{\mathbf{ERV}}_D = \left[\underline{ERV}_{1D}\ \underline{ERV}_{2D} \cdots \underline{ERV}_{QD}\ \underline{ERV}_{(Q+1)D} \right]^T, \end{cases} \tag{12}$$

where $\underline{\mathbf{ERV}}_U$ and $\underline{\mathbf{ERV}}_D$ are the feature vectors of h_{u} and h_{d}, respectively, $\underline{\mathrm{ERV}}_{JU}$ and $\underline{\mathrm{ERV}}_{JD}$ $(J = 1,2, \ldots, (Q+1))$ are the energy ratios of feature bands respectively, and $\underline{ERV}_{(Q+1)U} = 1 - \sum_{J=1}^{Q} \underline{ER}_{JU}$, $\underline{ERV}_{(Q+1)D} = 1 - \sum_{J=1}^{Q} \underline{ER}_{JD}$.

Based on $\underline{\mathbf{ERV}}_U$ and $\underline{\mathbf{ERV}}_D$, energy ration deviation of a feature band ERD_K can be expressed as

$$ERD_K = \left| \underline{ERV}_{KU} - \underline{ERV}_{KD} \right| (K = 1,2,\ldots,Q,Q+1). \tag{13}$$

Then, the Wavelet Packet damage feature vector **ERD** is created and expressed as

$$\mathbf{ERD} = \left[ERD_1\ \ ERD_2\ \ \cdots\ \ ERD_Q\ \ ERD_{Q+1} \right]^T. \tag{14}$$

The fluctuation degree of energy ratios on the feature bands can be reflected via the **ERD**. The energy ratios on the feature bands are not changed, when the **ERD** is a zero vector. In contrast, the energy ratios on the feature bands are changed, when the **ERD** is a nonzero vector. The **ERD** is a zero vector, when the wind-break wall is undamaged, and the **ERD** is a nonzero vector, when the wall is damaged. Thus, the damage state can be detected via the **ERD**.

2.2. Damage Identification Index. Based on the **ERD**, a damage identification index (Energy Ratios Variation Coefficient of the feature bands) is defined and expressed as

$$ERVC = \sqrt{\sum_{K=1}^{Q+1} \left(\frac{\underline{ERD}_K}{\underline{ERV}_{KU}} \right)^2}. \tag{15}$$

The value of *ERVC* is nonnegative. The value of *ERVC* is zero, when the energy ratios of the feature bands are not changed. Thus, the wind-break wall is undamaged. In contrast, the value of *ERVC* is positive, when the energy ratios of the feature bands are changed. Thus, the wind-break wall is damaged. The value of *ERVC* becomes much larger, when the accumulated damage becomes much bigger. In addition, the damage will cause stiffness changes of the wind-break wall, which will cause changes of dynamic responses to the wind-break wall. This will result in variations of *ERVC* which is based on the VIRF. The stiffness changes in the partial damage are the largest, and the change of *ERVC* value is the biggest in the partial damage too. Thus, the position where the value of *ERVC* is the biggest is the most close to the partial damage. Thus, the damage location of partial damage can be diagnosed via analyzing the characteristics of *ERVC* values. With increase of the damage intensity, the *ERVC* value increases continuously. The damage intensity can be calculated reversely via *ERVC*, if the quantitative relationship between the damage intensity and *ERVC* is known. Thus, the partial damage intensity can be identified via the quantitative relationship between the damage intensity and damage index.

3. Tests Analyses

To verify the validity of this damage identification method, vibration tests on a pile plate wind-break wall (reinforced concrete wall) are performed. The geometrical parameters and material parameters of the wall are listed in Table 1. To obtain dynamic response signals, an impulse excitation is loaded on the wall via the DFC-2 hammer, as shown in Figure 1(a). The positions of excitation are from point I to point III, as shown in Figure 1(b). To collect the dynamic response signals, six sensors are fixed on the wall. The positions of sensors are from point 1 to point 6, as shown in Figure 1(b), and the sensors are 941B acceleration sensors (the frequency range of these sensors is 0.17~100 Hz, and the sensitivity is 0.3 V·s^2/m). The signals recorded via sensors are collected by the signal collecting system, the JM3863A wireless vibration test system. The signals collected by the JM3863A are transmitted to a computer by the JM1802 gateway. The 941B sensor, JM3863A wireless vibration test system, and JM1802 gateway are shown in Figure 2. In the light of literature [20], damage can be simulated via reducing the elasticity modulus (such as changing material), changing the cross-sectional area (such as drilling holes and reducing section dimension), and weakening connection performances. In this paper, holes are drilled in the wall to simulate damage, as shown in Figure 3, and the parameters of the holes are listed in Table 2. Generally speaking, the early damage will appear in partial area. With damage increase in partial area, the total structure tends to be destroyed. Here, the partial damage is simulated in the area with 0.0625 m^2, as shown in Figure 1(b). To define the partial damage intensity, *DI* (damage intensity) is introduced and expressed as

$$DI = \left(\frac{N \cdot V_h}{V} \right), \tag{16}$$

where N is the number of holes, V_h is the volume of a single hole, and V is the total volume of the partial area ($V = 0.25\ \mathrm{m} \times 0.25\ \mathrm{m} \times 0.1\ \mathrm{m}$). Seven damage cases are simulated to identify the damage within the wind-break wall, as listed in Table 3. Case 1 is the undamaged case, and cases 2 to 7 are damaged cases. With increase of the number of holes, the value of *DI* increases, as shown in Figure 4.

Table 1: The geometrical parameters and material parameters of the wind-break wall.

Geometrical parameters		Material parameters	
Height/m	2.2	Density/(kg/m^3)	2500
Length/m	3.0	Elasticity modulus/MPa	2.11×10^4
Thickness/m	0.2	Poisson' ratio	0.2
Anchored depth/m	0.6	Cohesive force/kPa	—
Distance between piles/m	0.9	Internal friction angle/°	—

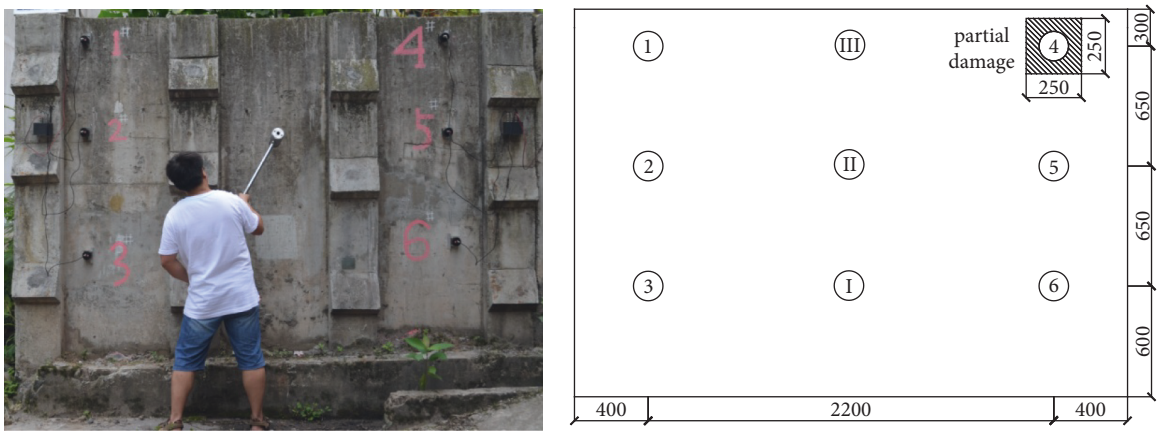

(a) (b)

Figure 1: Vibration tests on the pile plate wind-break wall. (a) Loading impulse excitation. (b) Position of the measurement points and partial damage.

(a) (b) (c)

Figure 2: Sensors, signal collecting system, and signal transmission system of vibration tests. (a) 941B sensor. (b) JM3863A vibration test system. (c) JM1802 wireless gateway.

Figure 3: Simulation of partial damage in the wind-break wall.

Table 2: The parameters of drilled holes.

Geometrical parameters	Unit
Diameter of a single hole	0.2 m
Depth of a single hole	0.1 m
Area of holes drilled	$0.25\ \text{m} \times 0.25\ \text{m} = 6.25\text{e}^{-2}\ \text{m}^2$
Scope of holes drilled	$\{L \in (2.475\ \text{m}, 2.725\ \text{m}), H \in (1.775\ \text{m}, 2.025\ \text{m})\}$

where L is the length of the wall and H is the height of the wall

Table 3: Damage cases.

Case	Case 1	Case 2 (%)	Case 3 (%)	Case 4 (%)	Case 5 (%)	Case 6 (%)	Case 7 (%)
DI	0	1.00	2.01	4.02	6.03	8.04	10.05

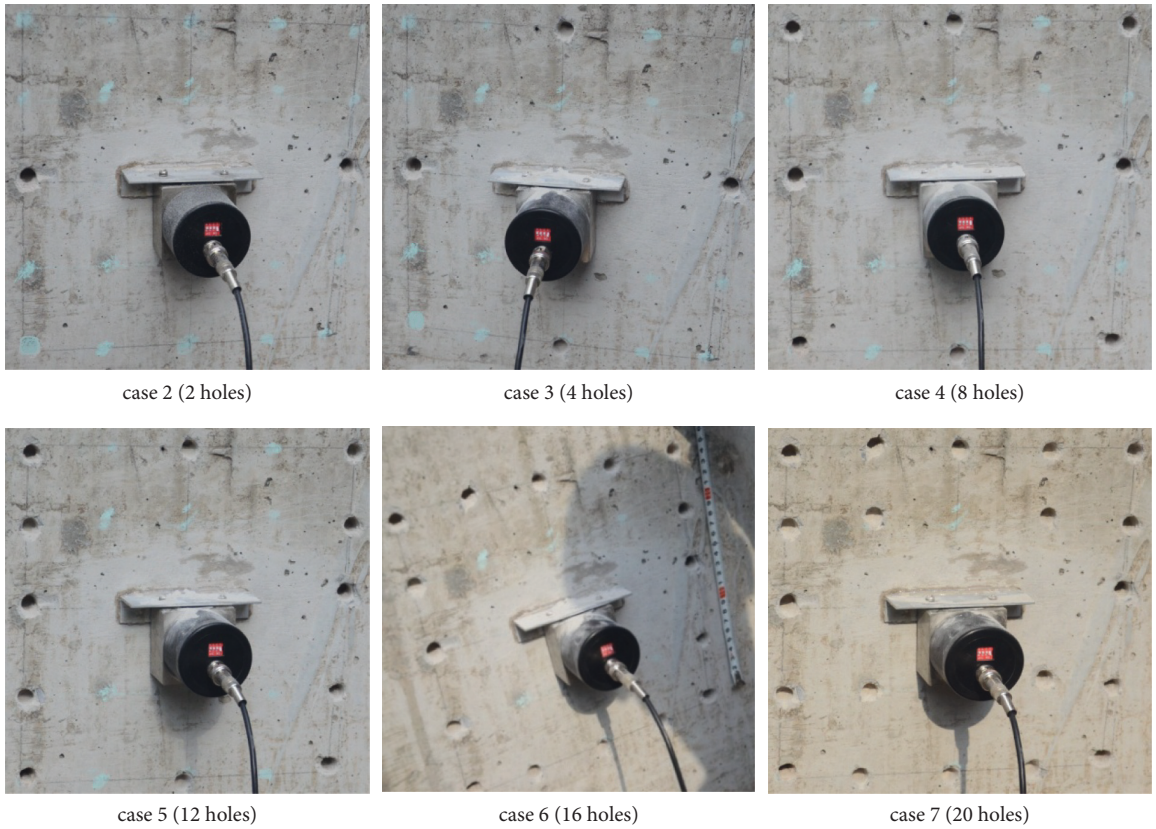

Figure 4: Partial damage: case 2 (2 holes), case 3 (4 holes), case 4 (8 holes), case 5 (12 holes), case 6 (16 holes), and case 7 (20 holes).

The test steps are as follows: (1) The wind-break wall is forced to vibrate under the hammer excitation. (2) The dynamic response signals are collected and transmitted to a computer. VIRF are acquired via data processing. (3) The Wavelet Packet frequency bands energy ratio spectrums are obtained via the Wavelet Packet Transform of VIRF. (4) The further updated Wavelet Packet frequency bands energy ratio spectrums are obtained. (5) The feature band vectors are created via analyzing the damage sensitivity of bands. (6) The damage feature vector and damage index are created and calculated. (7) The damage state of the wind-break wall is detected. (8) The damage location of the wind-break wall is diagnosed. (9) The damage intensity of the wind-break wall is identified.

To analyze the influences of excitation positions on the damage index, vibration tests are performed for three times at each excitation point under every damage case. In the light of literature [19], the measurement point with smaller response is selected as the virtual excitation point, and those measurement points with larger response are selected as virtual response points to obtain a better VIRF. In view of measurement point 3 with smaller response, point 3 is regarded as the virtual excitation, and five other measurement points are regarded as virtual responses. To select an optimal order of the Wavelet Packet decomposition and optimal wavelet basis function, after the Wavelet Packet decomposition of VIRF for many times, the analysis results are optimal when the Wavelet Packet decomposition (seven orders) of VIRF with Daubechies 18 wavelet basis function is performed. Thus, the wavelet basis function is selected as Daubechies 18, and the number of decomposition orders is seven.

3.1. Detecting the Damage State of the Wall. To eliminate the interference of measurement noise, the Wavelet Packet denoising of dynamic responses to the wind-break wall is performed under the hammer excitation. After the Wavelet Packet denoising of responses, it is found that only the signal within the first six minutes can be used to extract damage information effectively. Based on the signal processing of the signal within the first six minutes, VIRF are obtained. The time history curves of VIRF of different points under different cases are shown in Figure 5. Obviously, the time history curves of VIRF nearly overlap under different damage cases. Thus, it is difficult to extract damage information via the VIRF time history curves.

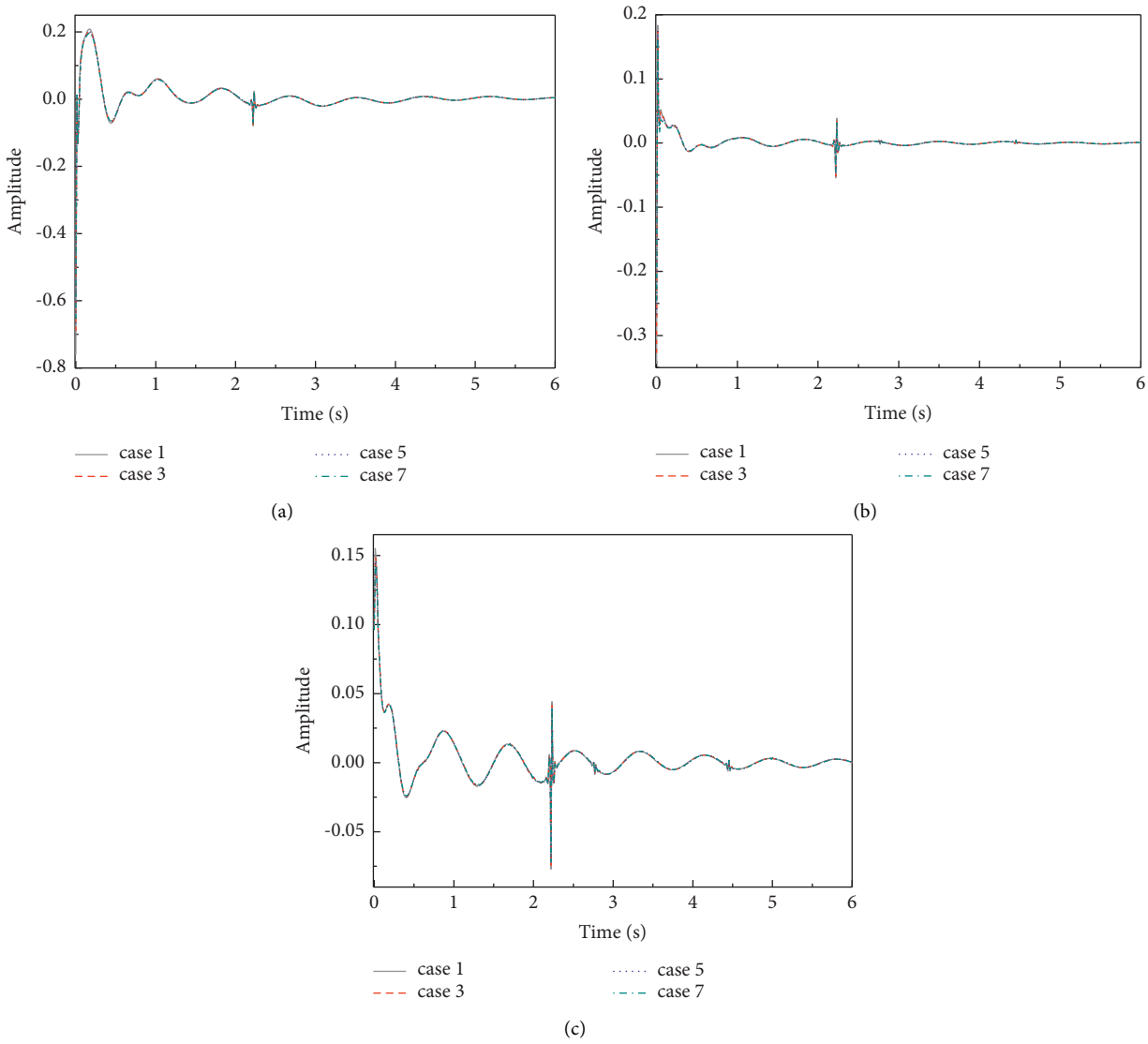

Figure 5: VIRF time history curves of measurement points (the second time test at excitation point II). (a) Point 4. (b) Point 5. (c) Point 6.

After the Wavelet Packet decomposition (seven orders) of VIRF with Daubechies 18 wavelet basis function, 128 subband energy ratios are acquired. As mentioned above, not each energy ratio of subband can be measured under such interferences as measurement noise, position of excitation, frequencies of excitation, and frequencies of the wind-break wall. The majority of energies are distributed on the minority bands with lower frequency, as shown in Figure 6. Here, only the first sixteen energies of subbands are exhibited. Taking point 5 as an example, the total energies of the first thirteen subbands are more than 99% of the total energies of energy ratio spectrum. Energies of the residual 115 subbands are nearly ignored, as shown in curves of Figure 7(b). Thus, the first thirteen subbands are useful for damage identification. With consideration of completeness of damage information, the residual 115 subbands are merged into one band (the fourteenth subband) via the threshold η_0. Then, the updated Wavelet Packet frequency bands energy ratio spectrum is acquired, as shown in Figure 7.

The relationship between η_0 and subband number is proportionate. With decrease of η_0, the number of subbands with larger energies also reduces, which may cause absence of damage information. With increase of η_0, the number of subbands with smaller energies also increases. However, the contribution of those subbands with smaller energies to damage identification is nearly neglected. Thus, addition of those subbands with smaller energies will reduce the efficiency of damage identification. The value of η_0 not only affects the number of subbands in the updated energy ratio spectrum but also affects the efficiency of damage identification. Thus, a reasonable value for η_0 should be considered. It is recommended that the value of η_0 should be in the range from 95% to 100%.

As mentioned above, the damage sensitivity of those bands with larger energies is not necessarily strong. To extract damage information sensitively, the further updated Wavelet Packet frequency bands energy ratio spectrums are obtained via sorting from strong damage sensitivity to weak

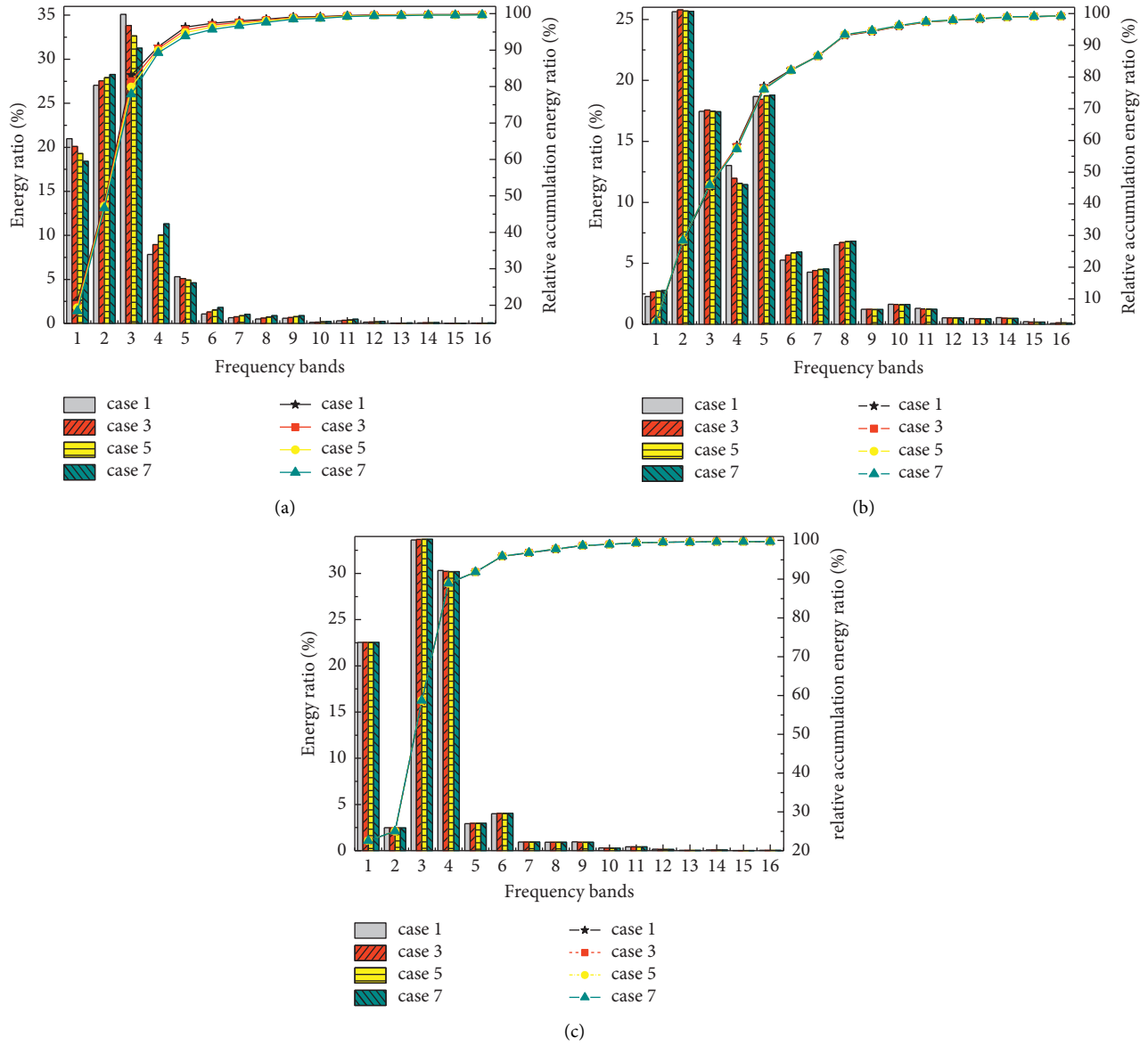

FIGURE 6: The frequency-ordered Wavelet Packet frequency bands energy ratio spectrum of different measurement points (the second time test at excitation point II). (a) Point 4. (b) Point 5. (c) Point 6.

one, as shown in Figure 8. The damage sensitivity of these bands with larger energy is much stronger in comparison with those bands with smaller energy. However, the energy of the band is much larger, and the damage sensitivity of this band is not necessarily stronger. Taking point 5 and point 6 as examples, the energy on the 6th band of point 5 and the energy on the 2nd band of point 6 are the largest, but the damage sensitivities of these two bands are not the strongest, as shown in Figures 8(b) and 8(c). In addition, the variation of damage intensity may cause changes of damage sensitivities to partial subbands. Taking point 5 as an example, with increase of the damage intensity, the damage sensitivities of the 4th band to the 8th band fluctuate greatly.

To improve the damage sensitivities of bands, these bands, which are much more sensitive to damage, are extracted from the further updated Wavelet Packet frequency bands energy ratio spectrums via the threshold ε_0, and the residual subbands are merged into the additional band. Then the feature bands are created. Based on the feature bands, the Wavelet Packet feature vector is created, as shown in Figure 9. From the curves in Figure 9, it is found that energies of these bands which are selected via ε_0 are nearly more than 95% of the total energies, which indicates that most of energies in the further updated energy spectrum are distributed on the bands selected via ε_0. In addition, the energies of feature vectors are also equal to the ones of the further updated Wavelet Packet frequency bands energy ratio spectrums. Thus, the feature vector, which can replace the further updated Wavelet Packet frequency bands energy ratio spectrums, can be used to identify damage within the wind-break wall sensitively.

The relationship between the threshold value ε_0 and number of feature bands is inversely proportional. With

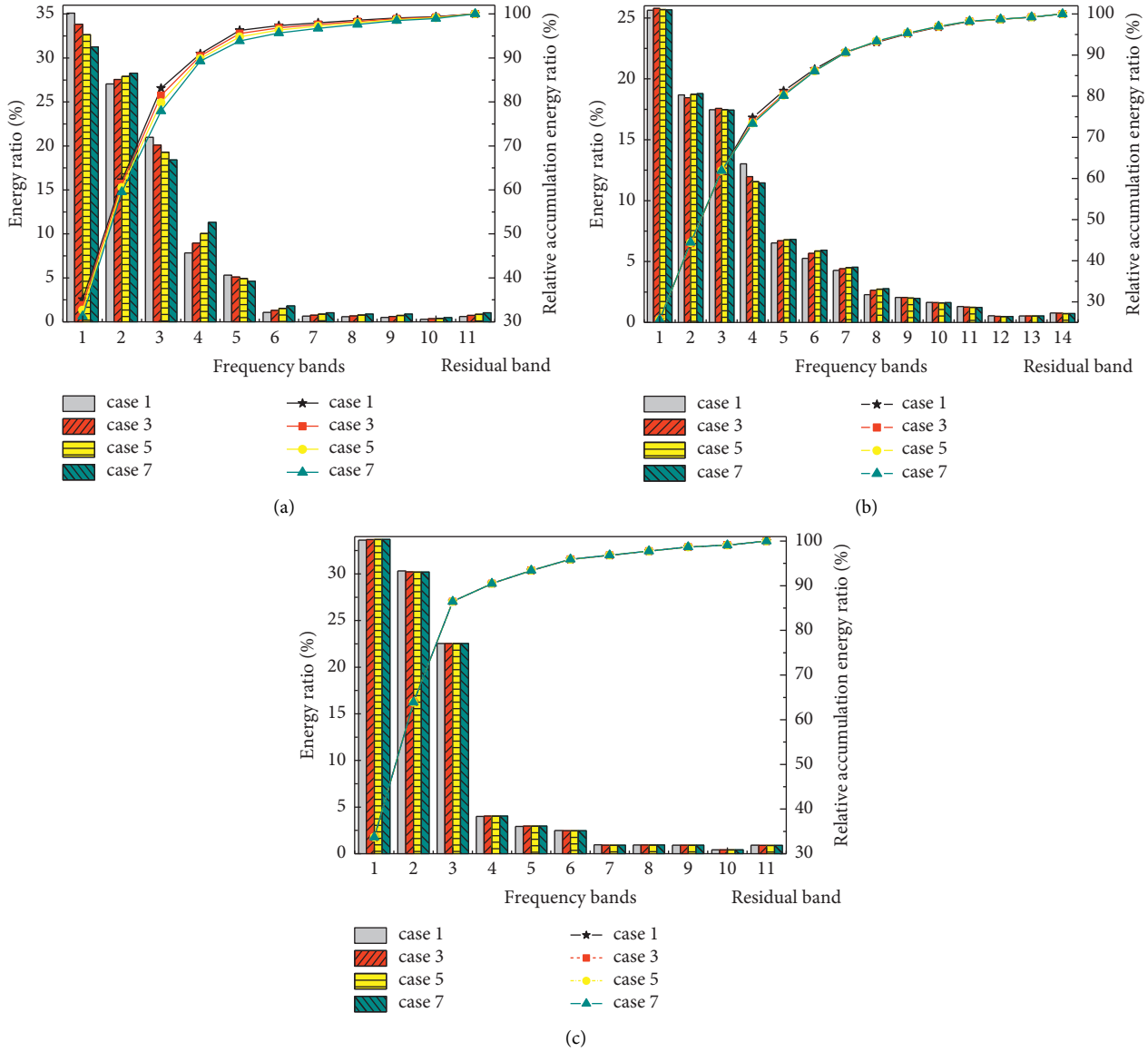

FIGURE 7: The updated Wavelet Packet frequency bands energy ratio spectrum of different measurement points (the second time test at excitation point II, $\eta_0 = 99\%$). (a) Point 4. (b) Point 5. (c) Point 6.

decrease of ε_0 value, the number of feature bands increases. This may cause the increase of the number of these bands with poorer damage sensitivity, which is not beneficial to damage identification. With increase of ε_0 value, the number of feature bands decreases. This may cause absence of some bands with stronger damage sensitivity, which results in absence of damage information. The value of ε_0 not only affects the number of feature bands but also affects the efficiency of damage identification. Thus, a reasonable value for ε_0 should be considered. It is recommended that the value of ε_0 should be in the range from 0 to 0.2.

Based on the feature vector, the Wavelet Packet damage feature vector is created, as shown in Figure 10. Obviously, the damage feature vectors are nonzero vectors. It is indicated that the wind-break wall is damaged. With increase of damage intensity, the fluctuation intensity of the damage feature vectors of different measurement points becomes larger and larger. Thus, the damage feature vector can be used to detect damage state of the wind-break wall. Under the influences of the excitation location and damage location, the damage sensitivities of different measuring points are different. The damage sensitivity of the point, which is much closer to partial damage, is much stronger. In contrast, the damage sensitivity of the point, which is far away from partial damage, is much weaker. Taking point 4 and point 6 as examples, the damage sensitivity of point 4 which is located in the partial damage is much stronger, while the one of point 6 which is far away from damage location is much poorer.

Based on the damage feature vector, the values of damage index of different measurement points are calculated under different damage cases, as shown in Figure 11(a).

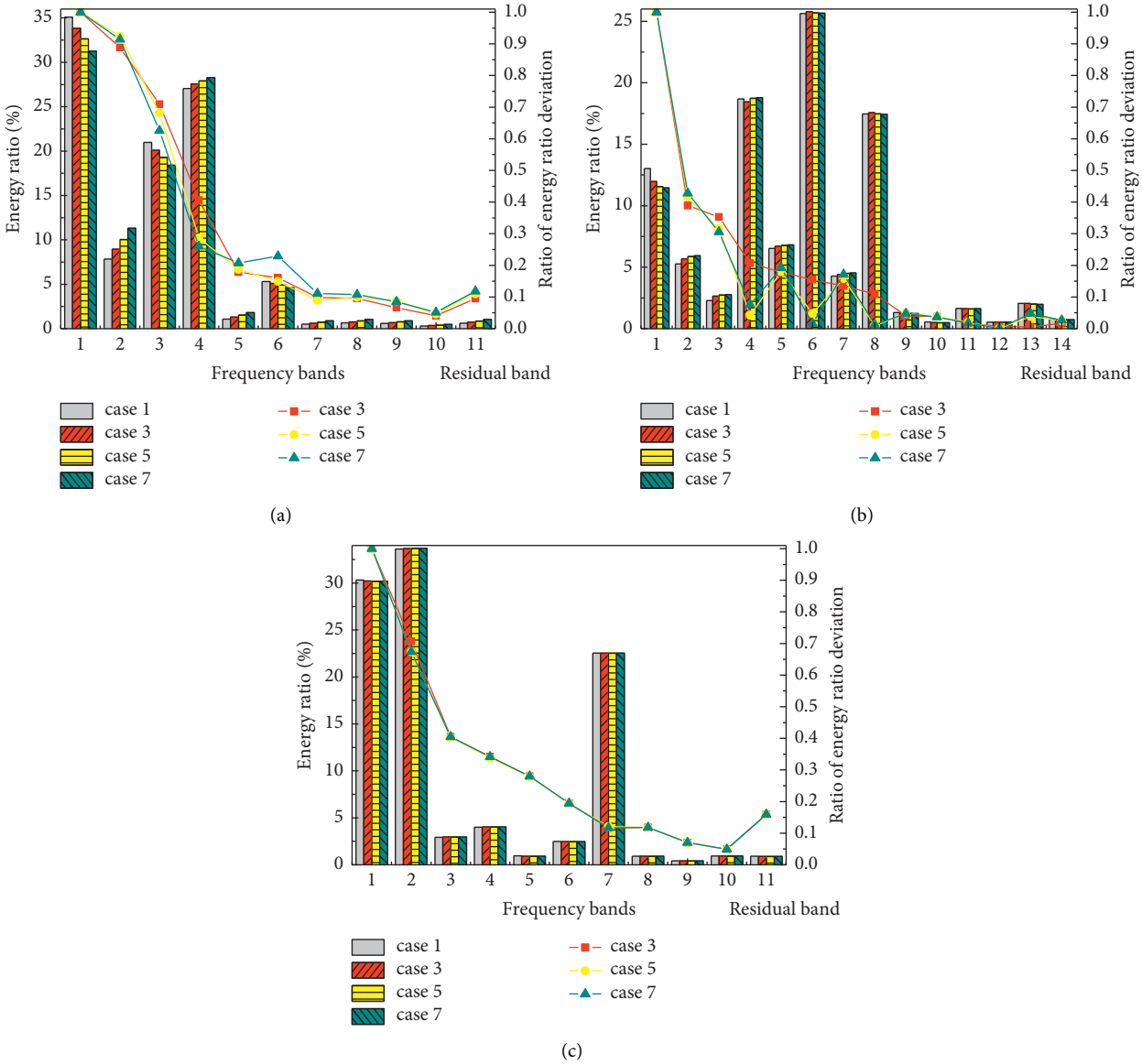

FIGURE 8: The further updated Wavelet Packet frequency bands energy ratio spectrum of different measurement points (the second time test at excitation point II). (a) Point 4. (b) Point 5. (c) Point 6.

With increase of damage intensity, the damage index values of measurement points also increase. Obviously, the damage state of the wind-break wall can be identified quantitatively via the values of damage index. Under the influence of location of partial damage, the damage index value of the point, which is closer to partial damage, is much larger under each damage case. For instance, the damage index value of point 4, which is located at the partial damage, is the largest. In contrast, the damage index value of point 6, which is far away from the partial damage, is much smaller, as shown in Figure 11(a). In addition, the amplifications of damage index value for different points are different under the influence of location of partial damage. To describe the amplification characteristics of damage index values, the slope curves of damage index curves are plotted, as shown in Figure 11(b). The slope of the damage index curve of the measurement point, which is much closer to partial damage, is much larger. For instance, the slope of the damage index curve of point 4, which is located at the partial damage, is the largest. The slope value of the damage index curve of point 4 is in the range from 14 to 33 under different cases. In contrast, the slope of the damage index curve of point 6, which is far away from the partial damage, is much smaller. The slope value of the damage index curve of point 6 is in the range from 0.4 to 3.5 under different cases. Thus, the damage location of the wind-break wall can be diagnosed via the characteristics of damage index curves. Besides, the efficiency of damage localization is poorer via the characteristics of damage index values, if every measurement point is far away from the partial damage. The efficiency of damage localization is the best, only when measurement points are assigned closely enough to the partial damage. Thus, whether the partial

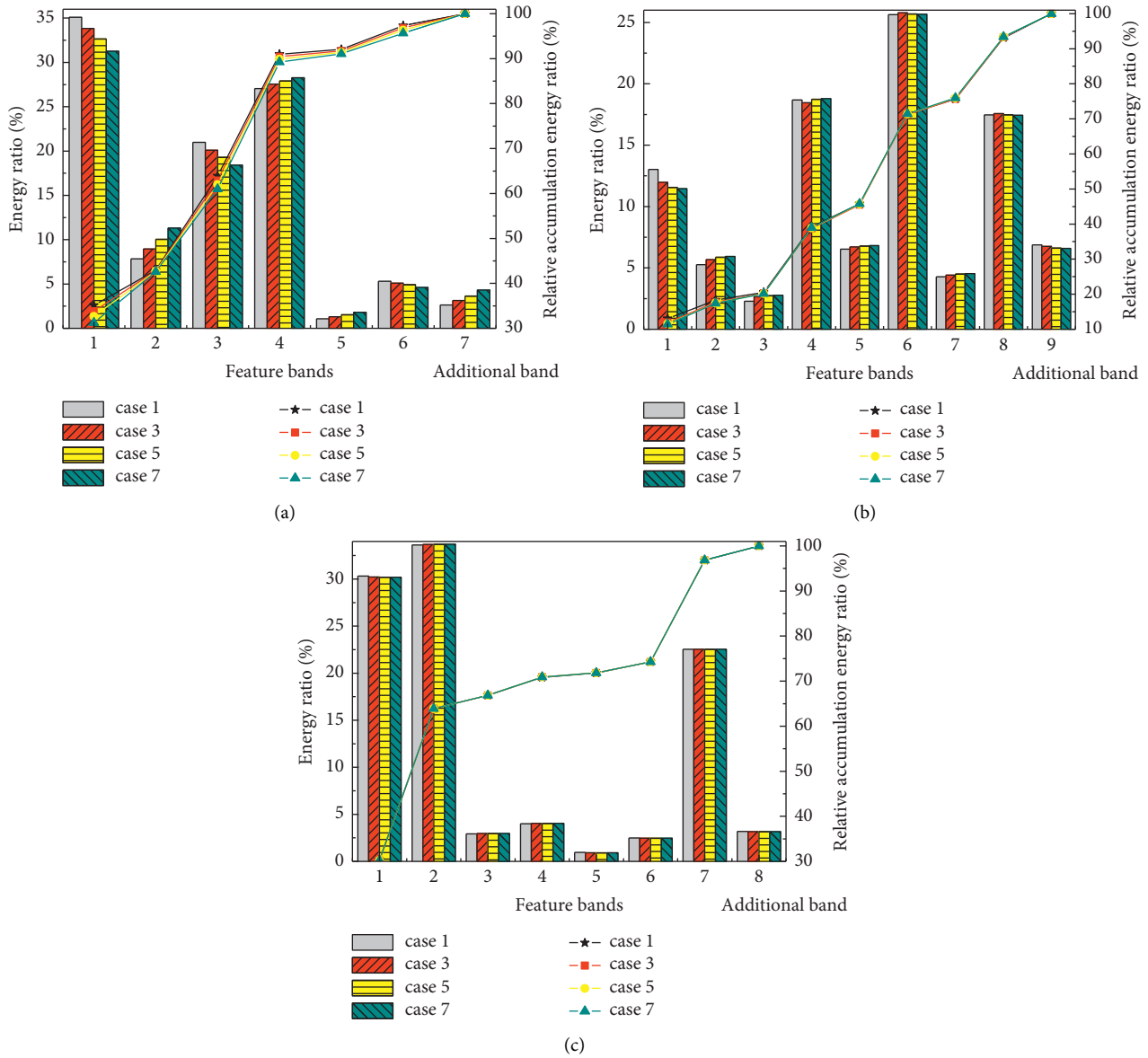

FIGURE 9: The Wavelet Packet feature vector of different measurement points (the second time test at excitation point II, $\varepsilon_0 = 0.1$). (a) Point 4. (b) Point 5. (c) Point 6.

damage can be diagnosed precisely depends on the distances between measurement points and partial damage area. In the light of literature [17, 20], 25 measurement points are assigned on the retaining wall model to localize damage. However, a larger number of measurement points are assigned on the practical structure with huge volume and big mass to localize damage, which will cause the cost increase greatly. Thus, adjusting locations of measurement points repeatedly may be economical and reasonable in practical engineering to localize damages.

The value of damage index changes when the location of hammer excitation changes. Thus, the location of hammer excitation has some influences on the damage index value. Taking point 4 as an example, the variance analysis of the damage index value is performed to describe this influence, as shown in Figure 12. The values of damage index are close under the different excitation location when the damage intensity is smaller. The variance values of damage index are also smaller. With increase of damage intensity, the variance values of damage index increase when the location of hammer excitation changes. Thus, with increase of damage intensity, the influence of excitation location on the values of damage index becomes larger and larger.

As mentioned above, the quantitative relationship between the damage intensity and damage index can be acquired via the polynomial fitting. Such problems as larger polynomial coefficient, larger degree of polynomial, and poorer fitting may occur, if the relationship between the damage intensity and damage index which is much larger than the value of damage intensity is fitted directly. Thus, the quantitative relationship between the relative damage

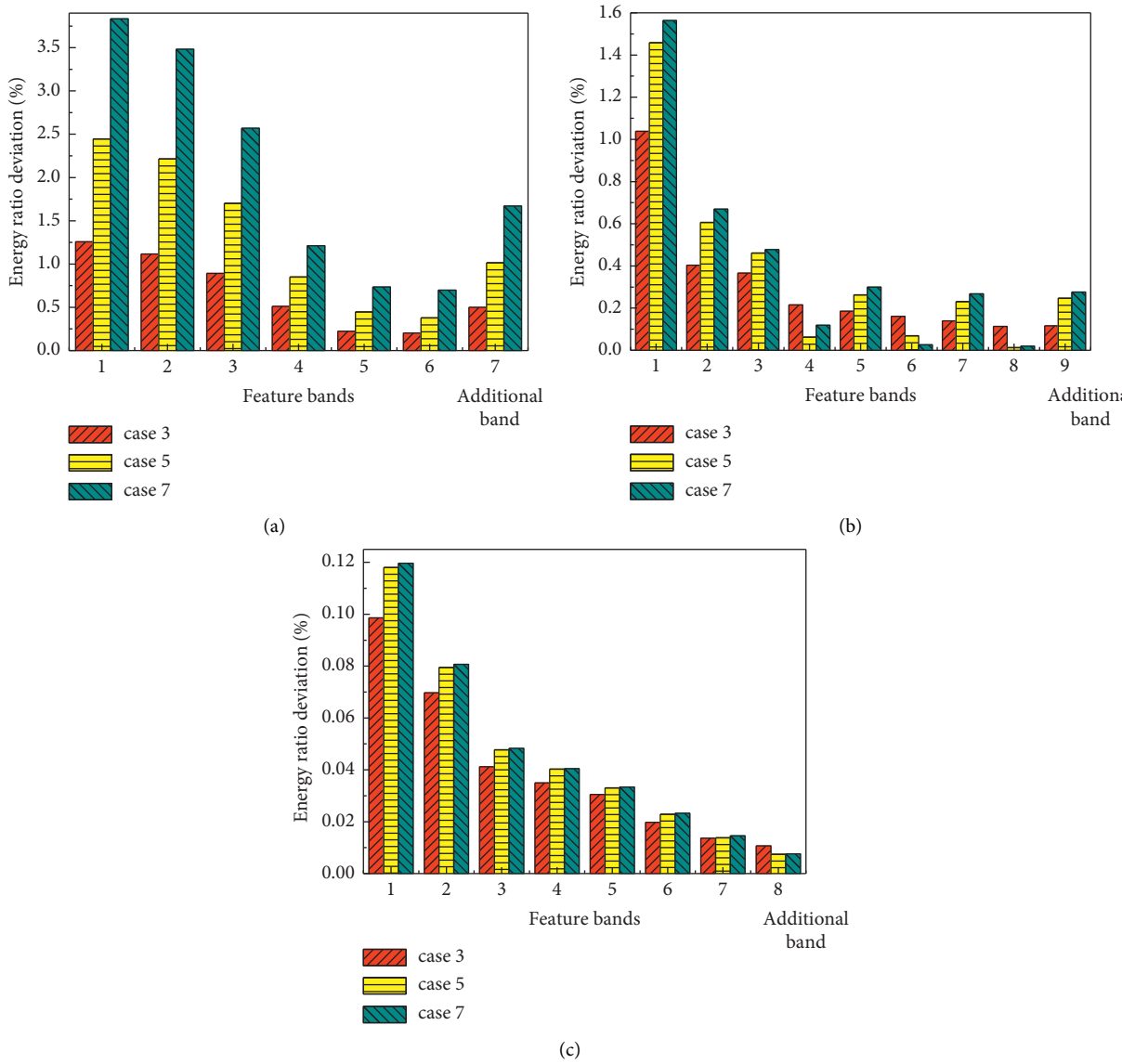

Figure 10: The Wavelet Packet damage feature vector of different measurement points (the second time test at excitation point II). (a) Point 4. (b) Point 5. (c) Point 6.

intensity and damage index value is fitted. Then, the quantitative relationships between relative damage intensity and damage index values are expressed as

$$\begin{cases} di = -15604x_1^4 + 6658x_1^3 - 682.63x_1^2 + 42.69x_1 + 0.014, \\ di = -210320x_2^4 + 49853x_2^3 - 3182.8x_2^2 + 92.62x_2 - 0.004, \\ di = 1.127x_4^5 - 5.81x_4^4 + 9.665x_4^3 - 5.358x_4^2 + 5.235x_4 + 0.05, \\ di = 1131.3x_5^5 - 1776x_5^4 + 991.2x_5^3 - 200.29x_5^2 + 22x_5 + 0.0095, \\ di = -1089100x_6^4 + 209140x_6^3 - 10911x_6^2 + 194x_6 + 0.0076, \end{cases} \quad (17)$$

where di ($di = DI \times 100$) is the relative damage intensity and $x_m (m = 1, 2, 4, 5, 6)$ is the mean value of ERVC of different measurement points for three times tests at different excitation points.

The quantitative relationships between relative damage intensity and damage index in equation (17) can be plotted as five fitting curves. Five tests curves can also be plotted via the tests. Each measurement point is corresponding to one group's curves, and each group's curves contain a test curve and fitting one. Five group curves, which are corresponding to five measurement points, are plotted, as shown in Figure 13. To describe the fitting degree of each group curves, the goodness of fit analysis for each group's curves is performed, and the value of coefficient of determination is used to describe the fitting degree of each group's curves. The value of coefficient of determination is much larger, and the fitting degree of the test curve and fitting curve is much better. Here, the coefficient of determination values of each group's curves are in the range from 0.93 to 0.95. Thus, fitting degree of each group's curves is better. However, the polynomial coefficient values of those points, which are far away from the partial damage area, are much larger, as listed in equation (17). Due to larger polynomial coefficient, the fitting precision becomes poorer, and the identification

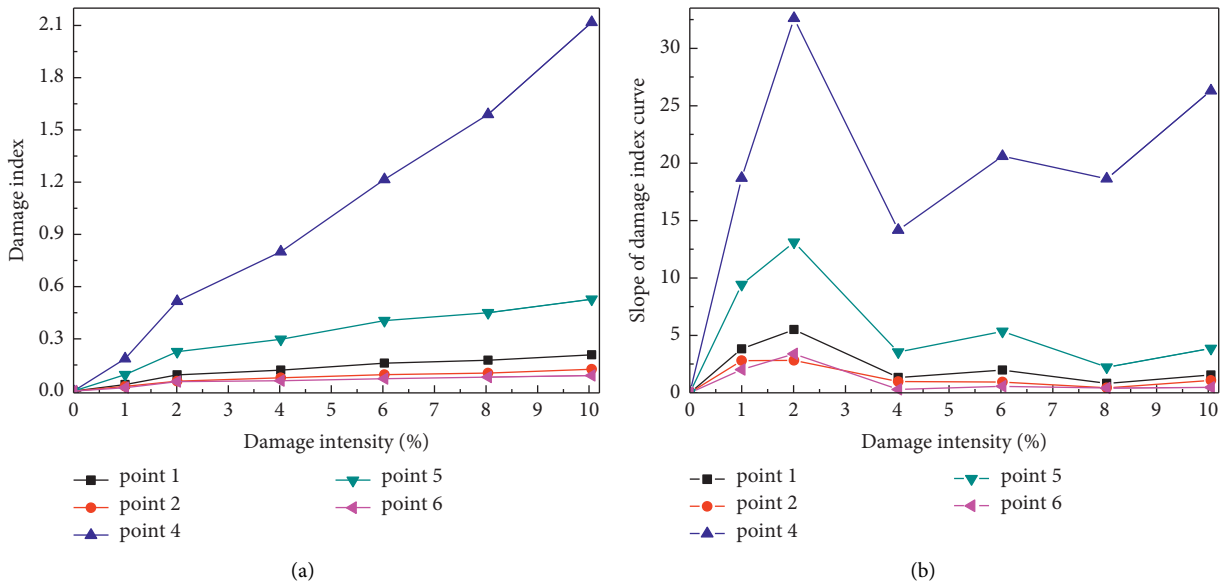

Figure 11: The relationship curves of damage intensity between damage indexes of different measurement points (the second time test at excitation point II). (a) Curves of damage index. (b) Slopes of damage index curves.

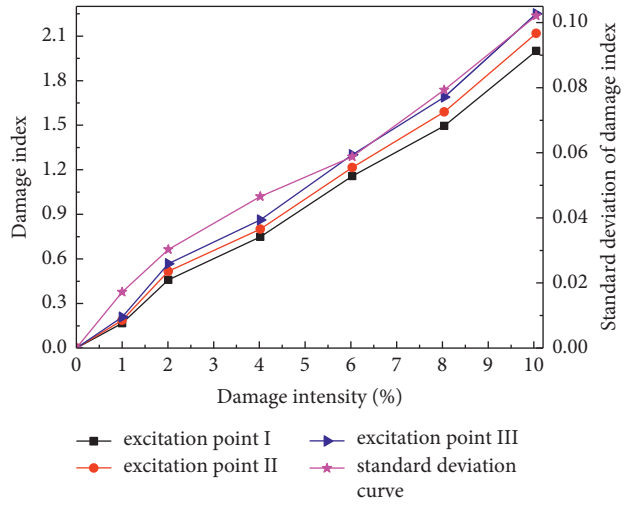

Figure 12: Curves of the damage intensity and damage index under different excitation points (point 4).

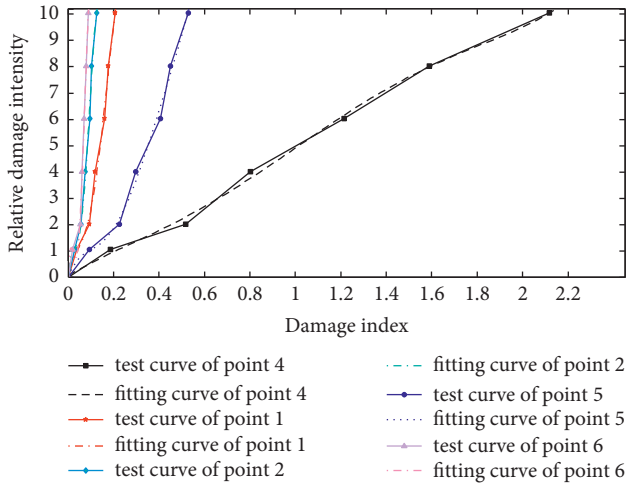

Figure 13: The relationship curves of damage intensity between damage indexes of point 4.

efficiency of damage intensity is poorer too. In contrast, the polynomial coefficient values of the point, which is close to the partial damage area, are much smaller. To ensure better fitting precision and identification efficiency, the damage intensity of the wind-break wall is identified via the quantitative relationship between the damage intensity and damage index values of point 4 which is located at the partial damage area. Then, the damage intensity can be calculated reversely, when the damage index is known. For instance, $di = 4.909$, when $ERVC = 1$. Thus, $DI = di/100 = 4.909\%$. Thus, the partial damage intensity of the wind-break wall can be identified via the quantitative relationship.

4. Conclusions

In this paper, based on the Wavelet Packet decomposition of VIRF of responses to the wind-break wall, the Wavelet Packet frequency bands energy ratio spectrum analyses of VIRF are performed. The further updated Wavelet Packet frequency bands energy ratio spectrum is proposed via the damage sensitivity analysis of subbands. Then, the feature bands which are more sensitive to damage are selected via the threshold value ε_0. Based on the feature bands, the damage feature vector, which can reflect damage information sensitively, is created. Based on the damage feature vector, a damage index is proposed. The wind-break wall is damaged, if the damage feature vector is a nonzero vector or the value of the damage index is positive. The partial damage can be localized via the variation characteristics of damage index. The damage intensity of the wind-break wall can be identified via the quantitative relationship between the damage index and damage intensity. Then, a damage identification method for wind-break wall is proposed, and damage within a wind-break wall is identified via this method. The results indicate that the wall is damaged when the damage feature vector is a nonzero vector. The damage can be localized by the measurement point whose damage index value is the largest. The damage intensity can be identified via the quantitative relationship between the damage index and damage intensity. Thus, the damage state, damage location, and damage intensity of the wind-break wall can be identified via this method, and this method is also suitable for such solid-web structures or components as building structures, bridge structures, retaining structures, plates, beams, and columns. However, this method may be unsuitable for lattice structures or components.

The number of bands in the further updated Wavelet Packet frequency bands energy ratio spectrum is determined by the threshold value η_0. With decrease of the value of η_0, the number of bands decreases too, which may cause loss of some bands with stronger damage sensitivity. Thus, the value of η_0 should be larger to avoid loss of those bands with stronger damage sensitivity. Additionally, the threshold value ε_0 has bigger influences on the number of feature bands. With increase of the value of ε_0, the number of feature bands decreases, which may cause loss of some bands with stronger damage sensitivity. To collect enough damage information, the value of ε_0 should be smaller. Either the η_0 value or the ε_0 value has influences on extracting damage information.

Thus, the values of η_0 and ε_0 should be reasonable. How to select reasonable values for η_0 and ε_0 needs to be considered in the future.

In this paper, such early damage types as microfracture and microholes are identified via this method. Whether such later damage types as plastic deformation and structural slide can be diagnosed via this method is still studied further. In addition, the wind-break wall is forced to vibrate due to such low strain excitation as hammer excitation. Under the effects of low strain excitation, dynamic responses to the wind-break wall can be regarded as linear ones. However, the responses to the wall may be nonlinear, when such ambient excitations as wind loads, blast loads, and seismic loads are loaded on the wall. Besides, the adaptation of the Wavelet Packet Transform to nonlinear responses is much poorer, which may affect the efficiency of damage identification. Thus, this method may be unsuitable for the structures with nonlinear responses.

Under the influences of excitation position, distance between measurement point and partial damage, inherent frequencies of wind-break wall, and excitation frequencies, the damage sensitivities of measurement points are affected. In the light of test results, those points with strong damage sensitivity have larger contribution to detecting damage state and diagnosing damage location. To improve damage sensitivities of measurement points, enough points should be assigned or locations of points should be adjusted repeatedly. In addition, the test data has larger influences on identifying damage intensity. The test data is more sufficient, and the precision of the quantitative relationship between damage intensity and damage index is better, which makes the damage identification efficiency better. Thus, to improve the precision of identifying damage intensity, collecting sufficient test data is required.

Data Availability

The data used are included in this paper. Based on the tables and figures in this paper, the readers can verify the results of this paper, replicate the analysis, and conduct secondary analyses.

Conflicts of Interest

The author does not have any conflicts of interest regarding the publication of this paper.

Acknowledgments

This paper was finalized by the National Natural Science Foundation of China (no. 51908345), Key Program of Social Development by Shaanxi Provincial Science and Technology Department (no. 2020SF-430), and Scientific Research Programs Funded by Shaanxi Provincial Education Department (I7JK0157 and 20JK0559).

References

[1] F. H. Liu, "Wind-proof effect of different kinds of wind-break walls," *Journal of Central South University*, vol. 37, no. 1, pp. 176–182, 2006.

[2] X. M. Pan, X. Q. Ma, and J. Xu, "Analysis and evaluation about anti-wind efficiency of wind break experimental section in Lan-Xin high railway," *Journal of Arid Meteorology*, vol. 37, no. 3, pp. 496–499, 2019.

[3] H. Q. Tian, "Research progress in railway safety under strong wind condition in China," *Journal of Central South University*, vol. 41, no. 6, pp. 2435–2433, 2010.

[4] K. Li, X. F. Liang, and M. Z. Yang, "Anti-wind aerodynamic performance of high-speed train and wind-break wall optimization," *Journal of Central South University*, vol. 49, no. 5, pp. 1297–1304, 2018.

[5] F. Han, L. Shi, and K. C. Liu, "Response law of wind-sand flow to windbreak wall along Lanzhou-Xinjiang high speed railway," *China Railway Science*, vol. 40, no. 5, pp. 9–15, 2019.

[6] G. W. Xin, N. Huang, and J. Zhang, "Wind-tunnel experiment on sand deposition mechanism and optimal measures of wind-break wall along railway in strong wind area," *Chinese Journal of Theoretical and Applied Mechanics*, vol. 52, no. 3, pp. 635–644, 2020.

[7] J. J. Cheng, J. Q. Lei, S. Y. Li, and H. F Wang, "Disturbance of the inclined inserting-type sand fence to wind-sand flow fields and its sand control characteristics," *Aeolian Research*, vol. 21, pp. 139–150, 2016.

[8] K. Ye and R. X. Li, "Optimization analysis of height and distance of shelter wind wall for high-speed railway," *Journal of South West Jiaotong University*, vol. 49, no. 2, pp. 240–246, 2014.

[9] B. Niu and L. M. Du, "Influence of sandstorms on the setting of wind-break wall of high-speed railway," *Journal of Railway Science and Engineering*, vol. 13, no. 8, pp. 1457–1465, 2016.

[10] S. Martin, G. Marcus, and M. Steffen, "A precise non-destructive damage identification technique of long and slender structures based on modal data," *Journal of Sound and Vibration*, vol. 365, pp. 89–101, 2016.

[11] Y. Z. Fu, Z. R. Lu, and J. K. Liu, "Damage identification in plates using finite element model updating in time domain," *Journal of Sound and Vibration*, vol. 332, no. 26, pp. 7018–7032, 2013.

[12] X. Z. Zhang, W. J. Yao, and B. Chen, "Damage identification of piles based on vibration characteristics," *The Scientific World Journal*, vol. 2014, Article ID 150516, 2014.

[13] H. Li, "The application of improved genetic algorithm on damage identification for frame structure," *International Journal of Control and Automation*, vol. 9, no. 2, pp. 229–238, 2016.

[14] C. Wang, C. P. Huang, and D. M. Ai, "Structural health alarming based on statistical wavelet packet energy distribution," *Journal of Civil Engineering and Management*, vol. 33, no. 6, pp. 12–15, 2016.

[15] Y. B. Jiao, H. B. Liu, and Y. C. Cheng, "Damage identification of bridge based on Chebyshev polynomial fitting and fuzzy logic without considering baseline model parameters," *Shock and Vibration*, vol. 2015, Article ID 187956, 2015.

[16] H. B. Liu, X. Q. Wang, and Y. F. Gong, "Damage identification of urban overpass based on hybrid neurogenetic algorithm using static and dynamic properties," *Mathematical Problems in Engineering*, vol. 2015, Article ID 404675, 2015.

[17] Q. Xu, "Damage identification investigation of retaining wall structures based on a virtual impulse response function," *Shock and Vibration*, vol. 2016, Article ID 1346939, 2016.

[18] T. Liu, A. Q. Li, Y. L. Ding, Z. Li, and Q. Fei, "Experimental study of the structural damage alarming method based on wavelet packet energy spectrum," *Journal of Vibration and Shock*, vol. 28, no. 2, pp. 4–9, 2009.

[19] A. Q. Li and Y. L. Ding, *Engineering Structures Damage Alert Theory and Application*, pp. 36-37, Science Press, Beijing of China, 2006.

[20] Q. Xu, "Damage index analysis of retaining wall structures based on the impulse response function and virtual impulse response function," *Shock and Vibration*, vol. 2021, Article ID 9741732, 2021.